

Frequency Encoding for Simultaneous Display of Multimodality Images

Mario Quarantelli, Bruno Alfano, Michele Larobina, Enrico Tedeschi, Arturo Brunetti, Eugenio M. Covelli, Andrea Ciarmiello, Ciro Mainolfi and Marco Salvatore

National Council of Research, Center for Nuclear Medicine, Naples; Department of Biomorphological and Functional Sciences, University Federico II, Naples; and Department of Nuclear Medicine, Fondazione G. Pascale, Naples, Italy

An original method for simultaneous display of functional and anatomic images, based on frequency encoding (FE), merges color PET with T1-weighted MR brain images, and grayscale PET with multispectral color MR images. A comparison with two other methods reported in the literature for image fusion (averaging and intensity modulation techniques) was performed. **Methods:** For FE, the Fourier transform of the merged image was obtained summing the low frequencies of the PET image and the high frequencies of the MR image. For image averaging, the merged image was obtained as a weighted average of the intensities of the two images to be merged. For intensity modulation, the red, green and blue components of the color image were multiplied on a pixel-by-pixel basis by the grayscale image. A comparison of the performances of the three techniques was made by three independent observers assessing the conspicuity of specific MRI and PET information in the merged images. For evaluation purposes, images from seven patients and a computer-simulated MRI/PET phantom were used. Data were compared with a chi-square test applied to ranks. **Results:** For the depiction of MRI and PET information when merging color PET and T1-weighted MR images, FE was rated superior to intensity modulation and averaging techniques in a significant number of comparisons. For merging grayscale PET with multispectral color MR images, FE and intensity modulation were rated superior to image averaging in terms of both MRI and PET information. **Conclusion:** The data suggest that improved simultaneous evaluation of MRI and PET information can be achieved with a method based on FE.

Key Words: brain; radionuclide studies; MRI; image display; image processing; PET

J Nucl Med 1999; 40:442-447

Image fusion is an attractive approach to multimodality diagnostic imaging. However, the techniques for simultaneous representation in a single image of functional (i.e., PET, SPECT, functional MRI and MR spectroscopic imaging) and anatomic (i.e., MRI and CT) information have not been assessed systematically. The ideal method for simultaneous display of multimodality images should provide a

single, "easy-to-read" image that holds all the relevant information contained in the original images.

Although there is no gold standard for fusion display, in most cases the low-resolution functional image is represented with an arbitrary color scale (pseudocolor) (1), which is often used to enhance intensity gradients within the image, and the high-resolution anatomic image with a grayscale. These two images are then averaged to obtain a transparency effect (or pseudo-transparency, if this effect is obtained using every other pixel from every other image) (2). This widely used technique is referred to here as image averaging (IA).

Another approach to image fusion has been proposed by Levin et al. (3), who suggested encoding the anatomic information using the local image intensity and functional information using color. This approach is referred to here as intensity modulation (IM).

Our working hypothesis was based on the fact that PET has a lower spatial resolution than MRI, so that its main information is contained in the low-frequency components of the image. This difference in frequency distribution of information can be used to fuse in the merged image the metabolic information (low frequencies) and the MR anatomic data (high frequencies). The use of Fourier transform (FT) may provide a way to combine these images more efficiently.

The aims of this study were twofold: (a) to develop a new technique for simultaneous display of anatomic and functional images based on frequency encoding (FE) of information; and (b) to assess the performance of this method, compared to IA and IM in merging the image sets under various experimental conditions.

The second step was performed using both MRI and co-registered ^{18}F -fluorodeoxyglucose (FDG) PET clinical brain studies and an original computer-simulated PET phantom. Finally, we compared the performance of the three different techniques for image fusion in merging pseudocolor PET and grayscale MR images, as well as grayscale PET and multispectral color images, obtained with an original post-processing procedure developed in our laboratory (quantitative magnetic color imaging [QMCI]) (4).

Received Mar. 26, 1998; revision accepted Aug. 3, 1998.
For correspondence or reprints contact: Mario Quarantelli, MD, Centro CNR per la Medicina Nucleare, Via Pansini 5, 80131 Napoli, Italy.

MATERIALS AND METHODS

MRI Studies

To obtain an adequate sampling of brain structures for accurate MRI/PET co-registration, MRI studies (1.5-T, Magnetom SP63; Siemens, Erlangen, Germany) were performed with sequential acquisition of two interleaved sets of oblique axial slices (15 slices per set, slice thickness 4 mm, slice interval 4 mm). Two spinecho sequences (repetition time [TR] = 600, echo time [TE] = 15; TR = 2300, TE = 15–90; both with 90° flip angle, 256 × 256 matrix, 0.98 mm pixel size) for each set of slices were acquired sequentially in the same spatial position. Slice positioning and angle were chosen on a sagittal localizer T1-weighted scan to cover the entire brain including cerebellum. For each slice, relaxation rate (R1 and R2) and proton density [N(H)] maps were computed, and the multispectral QMCI images, in which the red, green and blue (RGB) components of the image correspond to the R1, R2 and N(H) map, respectively.

PET

Brain PET studies were performed with a 47-slice scanner (ECAT EXACT 47; Siemens) 30 min after the intravenous administration of 185 MBq (5 mCi) FDG. In-plane spatial resolution was 6.3 mm (full width at half maximum [FWHM] at 10 cm from the slice center), slice thickness was 3.375 mm and pixel size was 2.81 mm. Axial images were obtained applying filtered backprojection (Hann filter with 0.4 frequency cutoff, 1.5 zoom factor) and calculated attenuation correction.

PET/MRI Co-Registration

The surface matching routine (5–7) of a commercially available software (Analyze TM Version 6.1.1; Mayo Biomedical Imaging Resource, Rochester, MN) was used for co-registration of the FDG PET and MRI studies. A three-dimensional rendering of the brain surface was provided by identifying the edge of the brain in the two sets of images using the interactive procedures available in the software package. The program calculated the translation, rotation and scaling parameters that minimize the mean square distance between the two surfaces. The process was repeated at increasing levels of precision and was stopped by the operator when the mean square distance reached consistency. After the registration, PET data were resliced onto the MR image coordinate system. Tri-linear

interpolation was used to produce PET slices with the same thickness as that of the original MR acquisitions.

Phantom

To assess the performance of the different simultaneous display techniques in controlled conditions, we generated a “virtual” single-slice PET phantom using identification of intracranial gray matter (GM), white matter (WM) and cerebrospinal fluid (CSF) in a brain MR scan by an automated segmentation procedure (8).

The following procedure was applied at the level of the basal ganglia to a segmented image of a 30-y-old healthy volunteer. GM/WM ratio and total true coincidences in our clinical studies were measured by averaging those obtained from the central slice in the patient PET studies. To obtain a GM/WM ratio for the phantom comparable to the clinical studies, GM of the segmented image was given an initial value four times higher than the WM value (Fig. 1A). All other tissues were zeroed.

Fifteen images with different pathologic distributions of activity were generated as follows. (a) Left hemisphere hypometabolism was simulated in 1 image by progressively decreasing the value of the pixels starting from the midline and reaching 40% of the original value in the leftmost cortex (Fig. 1B). (b) Six images simulating a necrotic area were obtained adding at the level of the right temporal lobe a circular area of hypometabolism with null activity in the center (Fig. 1C). Different lesion sizes were simulated using Gaussian profiles with a FWHM of 10, 16, 24, 31, 35 and 42 pixels. (c) Three images simulating a hypometabolic area were obtained adding at the level of the right temporal lobe a circular area of decreased values with a Gaussian profile (35 pixels FWHM). Different degrees of hypometabolism were simulated using a minimum value of activity in the center of the lesion of 40%, 60% and 80% of the original value. (d) Five images simulating a hypermetabolic area were obtained adding at the level of the right temporal lobe a circular area of increased values with a Gaussian profile (35 pixel FWHM, Fig. 1D). Different degrees of hypermetabolism were simulated using maximum increases of 6.2%, 12.5%, 25%, 37.5% and 50% of the original value. All final images were rescaled to a maximum value of 255.

To replicate the field of view of the PET scanner, the images obtained in the preceding steps were rebinned onto a 64 × 64 matrix. A scale factor of 0.08 was introduced to replicate the total

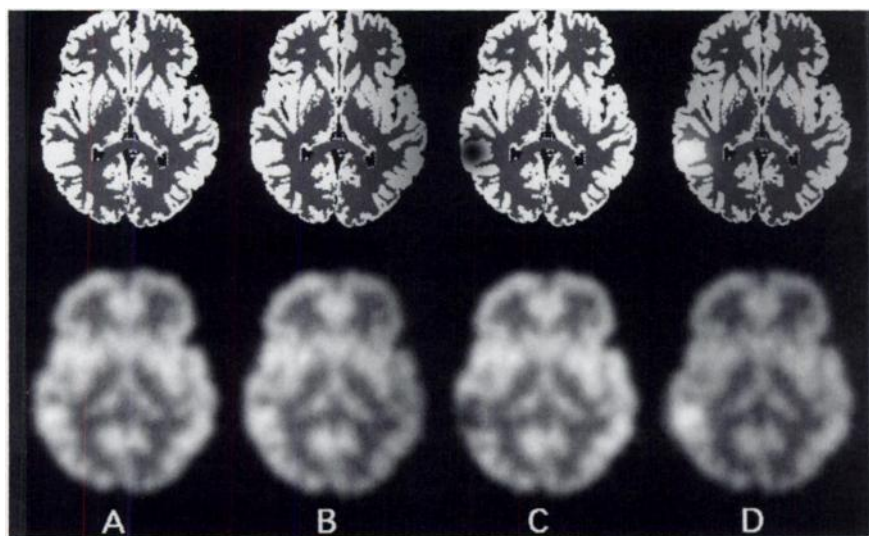


FIGURE 1. Normal distribution (A), left hemisphere hypometabolism (B) and examples of PET phantom with hypometabolic (C) (35 pixel FWHM, minimum intensity: 0% of GM value) and hypermetabolic (D) (35 pixel FWHM, maximum intensity: 150% of GM value) right temporal lesions. Top row: GM (intensity value 255) and WM (intensity value 64) maps used for phantom generation. Bottom row: resulting PET images. Each image is scaled to its own maximum.

true counts per sinogram in our PET studies. The corresponding emission sinograms with 190 views \times 160 angles were obtained. To simulate the detection angle error, a three-point smoothing filter was applied to the sinogram rows. To simulate photon attenuation, the segmented image including all head structures was used to obtain an attenuation sinogram. After rescaling to correct for pixel size, a temporary sinogram with 190 views \times 160 angles was obtained.

The final attenuation sinogram, assuming for the head a homogeneous linear attenuation coefficient of 0.088 cm^{-1} , was then generated as $e^{-0.0345 \times \text{sino}}$, where sino is the temporary attenuation sinogram. The emission sinograms were then multiplied by the attenuation sinogram.

Poisson-distributed noise was added to the resulting sinograms using Monte Carlo simulation. Measured attenuation correction was simulated dividing the emission sinogram by the final attenuation sinogram.

The same filtered backprojection algorithm used for the clinical PET studies (Hann filter with 0.4 pixel cutoff and 1.5 zoom factor) was applied to the sinograms to obtain the 16 final simulated PET images (1 with normal activity distribution and 15 with pathologic activity distribution). The GM/WM ratio (4:1) and the global scale factor (0.08) of the phantom generation were obtained by iterative adjustments.

Patients

PET and MRI studies were performed within a 6-h interval in seven patients with heterogeneous brain diseases with various PET and MR appearances (two cerebral toxoplasmosis, one lymphoma and four high-grade astrocytomas). In each patient, a single MR image acquired at the level of the lesion and the corresponding co-registered PET image were selected for the evaluation procedure.

Simultaneous Display Techniques

For simultaneous display, IA, IM and FE were implemented using the following techniques.

Image Averaging. A weighted average of the grayscale image with each of the RGB components of the corresponding color image provided the RGB components of the final merged image. The weight of the grayscale image (%Gray) can be changed to obtain the desired enhancement of the corresponding information, the weight of the RGB components being equal to $1 - \% \text{Gray}$. This technique has been applied to the pseudocolor PET/grayscale MR images combination (%Gray = 75%) and to the grayscale PET/QMCI combination (%Gray = 50%).

Intensity Modulation. To modulate the intensity of the pseudocolor PET using the T1-weighted image, as originally proposed by Levin et al. (3), the RGB components of the PET image are multiplied on a pixel-by-pixel basis by the grayscale T1-weighted image.

We have applied the same procedure to the RGB components of the QMCI image, modulating their intensity using the corresponding grayscale PET image. In both cases, an intensity windowing was performed (in our setting, 20% and 80% of the maximum value were chosen as optimal lower and upper window limits, respectively) to enhance the grayscale image information, because the use of color already increases the conspicuity of the color image information.

Frequency Encoding. Separation of the frequencies in which the relevant PET and MR information are contained can be used to fuse co-registered images, minimizing the loss of information in the merged image. This approach is schematically described, as applied to two grayscale images (PET and corresponding T1-weighted image), in

Figure 2. This procedure can be applied in turn to merge the RGB components of a color image and a grayscale image, given that the respective information reside in different frequency ranges.

The following procedure is used to merge pseudocolor PET and grayscale T1-weighted images. A high-pass filter is applied to the FT of the T1-weighted image, whereas a low-pass filter is applied to the FT of the RGB components of the pseudocolor PET. To preserve the relevant PET information, avoiding over- or underfiltering, as a low-pass filter for the PET FTs, we used a two-dimensional Gaussian function centered on the two-dimensional FT origin, with the same FWHM of the FT of the point spread function of the PET scanner (32 pixels). T1-weighted image was filtered using the complementary function as a high-pass filter.

The low-passed FT of the pseudocolor PET RGB components and the high-passed FT of the corresponding T1-weighted image were then summed, finally obtaining the RGB components of the merged image by inverse fast FT. The same technique was used to merge the grayscale PET with the QMCI images. MRI- and PET-filtered FTs were multiplied by the same weights used for the averaging method (%Gray = 75% for pseudocolor PET/grayscale MRI merging and %Gray = 50% for QMCI/grayscale PET merging).

These reported percentages and thresholds were selected by one of the authors, who did not participate in the subsequent evaluation.

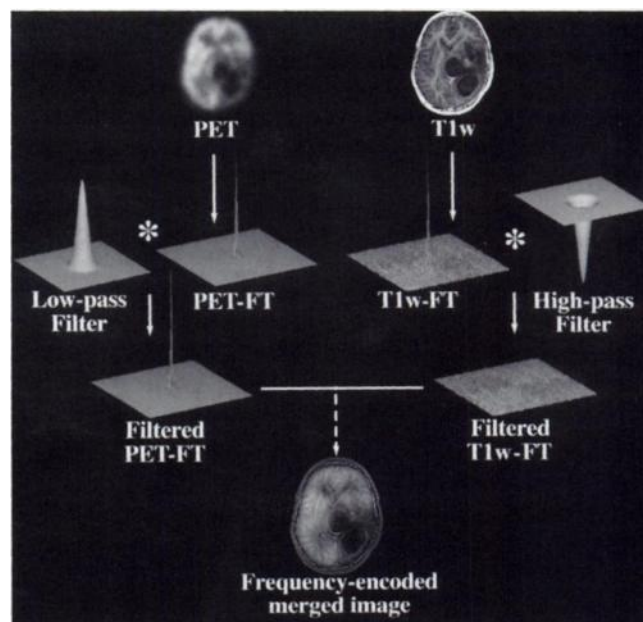


FIGURE 2. Diagram of FE technique in its simplest application, as applied to grayscale PET image and corresponding T1-weighted MR image. Note different composition in frequencies of FTs of PET (relevant information residing in central low-frequency peak) and of T1-weighted image (relevant information contained in "carpet" of high frequencies). Separation of frequencies in which relevant information reside is rationale for FE method. First, FT of two images to be merged are obtained by fast FT (long arrows). FTs are then multiplied (asterisks) by low-pass (PET image) or by complementary high-pass (MR image) filter function. Resulting filtered FTs are summed to obtain "hybrid" FT (not shown), which contains high frequencies of MR image and low frequencies of PET image. Finally, by applying inverse fast FT (dashed arrow), merged image represented in bottom row is obtained.

The optimal values were selected by iterative adjustment performed on the whole set of images and were subsequently applied to the merging processes of the other image sets. All programs for virtual PET phantom images generation and simultaneous display were written using Interactive Data Language (IDL; Research Systems, Inc., Boulder, CO) on a DEC-Alpha 200 workstation (Digital Equipment Corporation, Maynard, MA) running OSF/1.

Performance Assessment

Twenty-three sets of images (16 computer-simulated and 7 patient studies) were evaluated by three physicians experienced in both nuclear medicine and MRI. Each set consisted of an MR image (T1-weighted and QMCI image), the corresponding co-registered PET (patients) or simulated PET (phantom) image (in grayscale and pseudocolor), plus the corresponding merged images to be evaluated.

Evaluation was performed separately on two types of paired images: (a) pseudocolor PET and corresponding grayscale T1-weighted image (Fig. 3), and (b) grayscale PET and corresponding QMCI image (Fig. 4). Evaluators were requested to complete a form with scores ranging from 1 to 3 for conspicuity in each merged image of the following features: sulci, ventricular spaces, GM/WM contrast and basal ganglia definition (belonging to the MRI data), as well as PET abnormalities and the distribution of PET activity. In patient studies, an additional score was requested for the conspicuity of the MRI abnormality in the merged images.

Sulci, ventricular spaces, GM/WM contrast, basal ganglia and MRI abnormality scores were then pooled into a single group for a total of 294 comparisons. The same pooling was done for the two

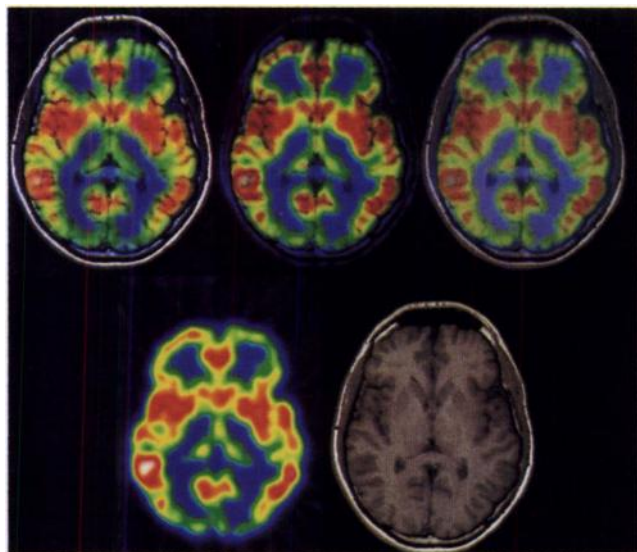


FIGURE 3. FE (top left), IM (top center) and IA (top right) merged images of pseudocolor PET (bottom left) and T1-weighted (bottom right) MR images of phantom with smallest hypermetabolic right temporal lesion (arrow, maximum value = 106% of normal GM). Note that use of arbitrary color scale introduces spatial gradients, resulting in artificial increase of high frequencies contained in RGB components of pseudocolor PET image. In this case, conspicuity of lesion is reduced in FE image, compared to other two techniques. Note also reduced definition of anatomic detail and presence of masking of anatomic detail in high-activity areas (basal ganglia and right temporal hypermetabolic lesion), more pronounced in IA image.

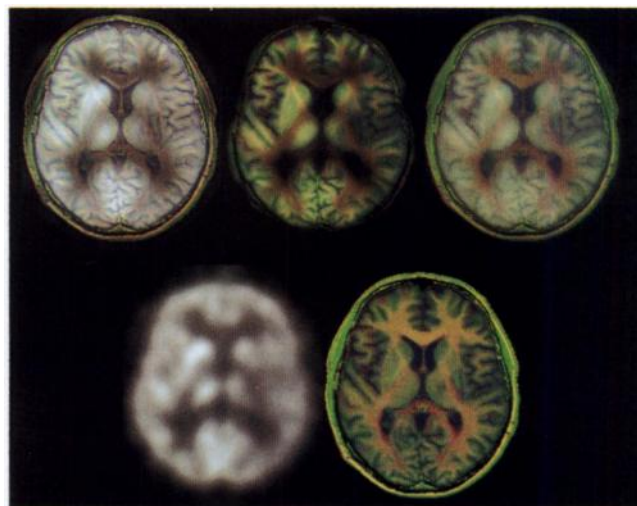


FIGURE 4. Bottom row: grayscale PET (left) and corresponding QMCI (right) images. Top row: merged images obtained using FE (left), IM (center) and IA (right) techniques. Slice at level of basal ganglia from study of patient with cerebral toxoplasmosis shows reduced glucose uptake at level of left hemisphere, with small hemorrhagic lesion at level of left posterior putamen (appearing green in QMCI image due to reduced R1 and increased R2), surrounded by mild edema (appearing purple). Another small area of edema (surrounding more caudal lesion, not shown here) can be seen at level of left thalamus.

PET features evaluated (135 comparisons). For each comparison between two merging techniques, scores were converted into ranks.

Statistical Analysis

The available techniques were compared separately for the MRI and PET features, using chi-square analysis applied to the pooled ranks from the three evaluators. We conservatively assumed as a null hypothesis equal distribution among the preferences in each comparison (first technique better than second, second technique better than first). Comparison was performed separately on each pair of techniques for the two image combinations (pseudocolor PET–grayscale T1-weighted image and grayscale PET–QMCI image). Significance threshold was set to 0.05. Bonferroni correction for multiple comparisons was applied.

RESULTS

The results of the comparisons of the different techniques are summarized in Table 1 (merging of pseudocolor PET with grayscale T1-weighted MR images) and Table 2 (merging of grayscale PET with QMCI MR images).

Pseudocolor PET–Grayscale T1-weighted MR Images. FE presented the best depiction of both MRI and PET information compared to IM and IA (Table 1).

Grayscale PET–QMCI MRI. When compared to IA, both IM and FE techniques better depicted MRI and PET information, whereas IM and FE did not present a significantly different performance from each other (Table 2).

DISCUSSION

We have shown the feasibility of merging PET and MR images using FE. Comparison with other techniques of

TABLE 1

Comparison of Three Simultaneous Display Techniques for Conspicuity of MRI and PET Information, Merging Pseudocolor PET and Grayscale T1-Weighted Images

	MRI (n = 294)			PET (n = 135)		
	1st	Equal	2nd	1st	Equal	2nd
FE vs. IM	156*	105	33	63*	51	21
IM vs. IA	132	57	105	39	45	51
FE vs. IA	144*	87	63	51*	69	15

* $P < 0.05$ (chi-quadro with Bonferroni correction).

FE = frequency encoding; IM = intensity modulation; IA = image averaging.

In MR images, evaluators looked at sulci, ventricular spaces, intracranial gray matter/white matter contrast, basal ganglia and lesion. In PET images, evaluators looked at overall distribution of activity and lesion.

n = total number of comparisons for the corresponding feature group. For each feature, the preferences given by the three evaluators to the first technique (left column), second technique (right column) or to neither (central column) are reported.

image fusion in a limited number of clinical and phantom images showed significantly superior performance by FE as compared to IA and IM in retaining relevant information in merged images. Different simultaneous display methods were reviewed by Rehm et al. (2), who proposed an interleaved pixel technique for optimal 8-bit color display of multimodality images. In the past few years, as higher performance hardware has reached lower costs, 24-bit color display has become an industrial standard even for low-end platforms, allowing an efficient simultaneous handling of multiple color scales.

It has been noted that the interleaved pixel technique suffers from a camouflage effect of the low-contrast details

TABLE 2

Comparison of Three Simultaneous Display Techniques for Conspicuity of MRI and PET Information, Merging Grayscale PET and Quantitative Magnetic Color Imaging

	MRI (n = 294)			PET (n = 135)		
	1st	Equal	2nd	1st	Equal	2nd
FE vs. IM	126	28	140	58	38	39
IM vs. IA	171*	35	88	79*	25	31
FE vs. IA	176*	103	15	98*	32	5

* $P < 0.05$ (chi-quadro with Bonferroni correction).

FE = frequency encoding; IM = intensity modulation; IA = image averaging.

In MR images, evaluators looked at sulci, ventricular spaces, intracranial gray matter/white matter contrast, basal ganglia and lesion. In PET images, evaluators looked at overall distribution of activity and lesion.

n = total number of comparisons for the corresponding feature group. For each feature, the preferences given by the three evaluators to the first technique (left column), second technique (right column) or to neither (central column) are reported.

of the MR image at the level of high PET activity regions. This finding, which appears to be due to perceptual merging of contiguous pixels, was confirmed using different combinations of test merged images (2). A similar effect also can be seen on the images merged with the IA technique, in which the corresponding pixels are actually averaged (Figs. 3 and 5). This phenomenon appears at least partially decreased in the FE images, due to the enhancement of the MR contrast in the final image as a result of the high-pass filtering (Fig. 5).

In addition, the selective preservation of the low-frequency PET information in the FE images allowed a better perception of the slightly hypermetabolic lesions in the grayscale PET/QMCI MR merging, compared to the other techniques (Fig. 5). However, when merging pseudocolor PET with grayscale MR images, FE performance is conditioned by the introduction of high frequencies in the pseudocolor PET image as a consequence of the use of an arbitrary color scale (Fig. 3). Therefore, when using FE, care should be taken not to use a color scale in which the RGB components vary too abruptly at any level.

It is noteworthy that FE can also be used to merge grayscale anatomic and functional images (Fig. 2), if the use of color needs to be avoided. In this case, IA and IM are expected to give clearly inferior results, because of the loss of information consequent to the simple averaging (IA) or multiplying (IM) of the two datasets.

IM provided a clearer picture of the MRI information in metabolically active tissues and allowed a good detectability of low-activity lesions. The major drawback of this tech-

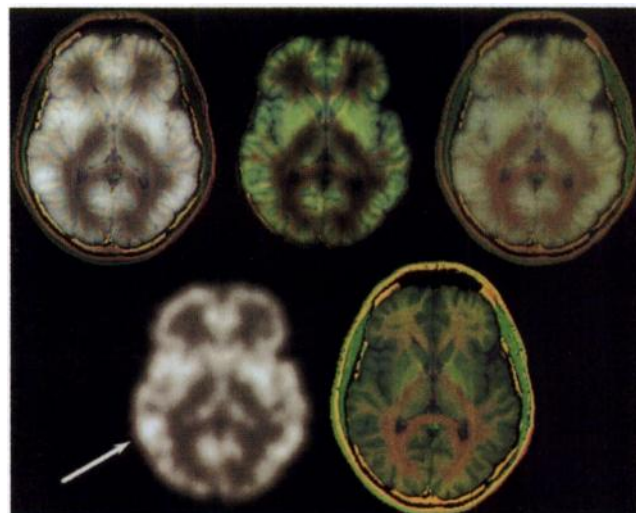


FIGURE 5. Same phantom as in Figure 3. Bottom row: grayscale PET image (left) and corresponding QMCI image (right). Top row: Merged images using FE (left), IM (center) and IA (right). Note loss of MRI detail (e.g., sulci definition) at level of high-activity areas in averaged image, which also shows least lesion conspicuity. Note excellent cortical anatomy definition in IM image, which, however, does not allow adequate assessment of anatomic details of regions with low PET activity (WM, CSF and extra-cerebral structures) and presents flattening of PET activity distribution due to compression of PET intensity scale.

nique, however, was the loss of anatomic detail in the low-activity areas, which did not allow the assessment of the anatomic features at the level of hypometabolic lesions and extracerebral structures. In addition, the compression of the PET scale to obtain a sufficient overall intensity of the image resulted in a flattening of the PET activity distribution in the merged images (Fig. 5).

We did not test systematically the performance of the merging techniques with MRI abnormalities, because their heterogeneity in terms of shape and signal alterations was such that a simulation could not be done using a virtual phantom.

It must be stressed that other low-resolution (SPECT, MR spectroscopic images) and high-resolution (CT) co-registered images can be fused using FE, appropriately varying the frequency filter to match the resolution of the functional images. This technique could also be used to merge images from studies of anatomic regions other than the brain.

CONCLUSION

The FE technique is proposed as an effective method for simultaneous display of functional PET and anatomic MRI information.

ACKNOWLEDGMENTS

The authors gratefully acknowledge the secretarial assistance of Ms. Carmela Imparato. This work was partially supported by an Italian Association for Cancer Research grant and by a grant from Regione Campania (L. 41/94).

REFERENCES

1. Pratt WK. *Digital Image Processing*. 2nd ed. New York, NY: John Wiley & Sons, Inc.; 1991:311–312.
2. Rehm K, Strother SC, Anderson JR, Schaper KA, Rottenberg DA. Display of merged multimodality brain images using interleaved pixels with independent color scales. *J Nucl Med*. 1994;35:1815–1821.
3. Levin DN, Pellizzari CA, Chen GTY, Chen CT, Cooper MD. Retrospective geometric correlation of MR, CT and PET images. *Radiology*. 1988;169:817–823.
4. Alfano B, Brunetti A, Arpaia M, Ciarmiello A, Covelli EM, Salvatore M. Multiparametric display of spin-echo data from MR studies of the brain. *J Magn Reson Imaging*. 1995;5:217–225.
5. Robb RA, Hanson DP. A software system for interactive and quantitative visualization of multidimensional biomedical images. *Australas Phys Eng Sci Med*. 1991;14:9–30.
6. Jiang H, Holton K, Robb R. Image registration of multimodality 3-D medical images by chamfer matching. *SPIE Biomed Image Processing Three-Dimensional Microscopy*. 1992;1660:356–366.
7. Jiang H, Robb RA, Holton K. A new approach to 3-D registration of multimodality medical images by surface matching. *SPIE Vis Biomed Comp*. 1992;1808:196–213.
8. Alfano B, Brunetti A, Covelli EM, et al. Unsupervised, automated segmentation of the normal brain using a multispectral relaxometric MR approach. *Magn Reson Med*. 1997;37:84–93.



The Journal of
NUCLEAR MEDICINE

Frequency Encoding for Simultaneous Display of Multimodality Images

Mario Quarantelli, Bruno Alfano, Michele Larobina, Enrico Tedeschi, Arturo Brunetti, Eugenio M. Covelli, Andrea Ciarmiello, Ciro Mainolfi and Marco Salvatore

J Nucl Med. 1999;40:442-447.


This article and updated information are available at:
<http://jnm.snmjournals.org/content/40/3/442>

Information about reproducing figures, tables, or other portions of this article can be found online at:
<http://jnm.snmjournals.org/site/misc/permission.xhtml>

Information about subscriptions to JNM can be found at:
<http://jnm.snmjournals.org/site/subscriptions/online.xhtml>

The Journal of Nuclear Medicine is published monthly.
SNMMI | Society of Nuclear Medicine and Molecular Imaging
1850 Samuel Morse Drive, Reston, VA 20190.
(Print ISSN: 0161-5505, Online ISSN: 2159-662X)

© Copyright 1999 SNMMI; all rights reserved.

 SOCIETY OF
NUCLEAR MEDICINE
AND MOLECULAR IMAGING